Solvent Reorganization Energy of Charge Transfer in DNA Hairpins

David N. LeBard,[†] Mark Lilichenko,[†] Dmitry V. Matyushov,*[,†] Yuri A. Berlin,[‡] and Mark A. Ratner[‡]

Department of Chemistry and Biochemistry and the Center for the Study of Early Events in Photosynthesis, Arizona State University, P.O. Box 871604, Tempe, Arizona 85287-1604, and Department of Chemistry and Center for Nanofabrication and Molecular Self-Assembly, Northwestern University, 2145 Sheridan Road, Evanston, Illinois 60208-3113

Received: June 2, 2003; In Final Form: October 18, 2003

We report calculations of solvent reorganization energies and the energy gap analysis for charge transfer in synthetic DNA hairpins consisting of two complementary strands linked by a stilbene chromophore. Reorganization energies are calculated for the processes of photoinduced hole injection from the linker to a neighboring guanine (G) through variable numbers of adenine/thymine (AT) pairs and for the hole transfer between adjacent G sites connected by AT bridges of different length. Twelve molecules with varying donor−acceptor separation have been analyzed. The solute structure is taken from crystallographic data with atomic resolution, and the polarization response of water is modeled in terms of polarization structure factors accounting for the molecular nature of the polarization fluctuations of the solvent. Both the magnitudes of reorganization energies and the parameter of the rate constant falloff with the donor−acceptor separation turn out to be much higher than those obtained from the Marcus-Levich-Jortner analysis of the experimental kinetic data. The discrepancy is resolved by applying a new model (Q-model) of charge-transfer accounting for different reorganization energies for charge separation and charge recombination reactions.

I. Introduction

The ability of deoxyribonucleic acid (DNA) to transport an excess charge over large distances has become the subject of intensive research since the key studies of Barton and collaborators.[1−3] Apart from vivid interest in gaining insight into the mechanism of charge migration in one of the basic biopolymers, current investigations are also driven by the implication of this phenomenon for the pathways of DNA oxidation damage,[4,5] mutations,[6−8] in the development of electrochemical biosensors,[9−11] and nanoelectronic devices.[12−19]

With several exceptions,[20−26] most experimental and theoretical studies have concentrated on understanding one-dimensional transport of a positive charge (the so-called electronic "hole") along the array of π-stacked Watson−Crick pairs in the interior of the double helix (for review see refs 27−37). According to the current consensus, the mechanism of charge motion is determined by the constraints imposed by different energetics of individual nucleobases, i.e., guanine (G), adenine (A), thymine (T), and cytosine (C). For instance, the hierarchy of oxidation potentials of the individual nucleobases in solution[38,39] and of the ionization potentials of nucleobases in duplexes[40] ($G < A \ll C, T$) allows the positive charge to be located essentially on G. Therefore hole motion in duplexes that are constructed of GC base pairs connected by AT bridges can be viewed as a series of hops between neighboring G sites serving as "resting states" for moving charge carriers.[41−43] Both experiment[44] and theory[45,46] show that the mechanism governing discrete steps of this motion crucially depends on the length of the AT bridge. For short bridges (up to 3 AT pairs), hole transfer between G bases occurs mainly due to quantum-mechanical tunneling, whereas transitions of positive charge over longer bridges require thermal activation.

The application of this mechanistic picture to theoretical analysis of steady-state experiments on DNA strand cleavage[42,47,48] has led to the formulation of a phenomenological model[49−53] of variable range hopping (VRH) in DNA. An obvious advantage of the VRH model is accurate predictions of both sequence and distance dependencies for the efficiency of hole transfer through stacks with various combinations of Watson−Crick base pairs.[52] This, in turn, provides a reasonable evaluation of the distance scale for the propagation of a positive charge in duplexes, which is needed to specify initiation of "chemistry at a large distance".[35] According to estimates,[51,52] the maximal distance traveled by holes in the course of their hopping motion in DNA can reach several hundred angstroms in accord with observations.[3,33,47,54]

It should be noted that information needed to predict sequence and distance dependencies for charge transport in DNA involves only the experimental data[42,44,48] on relative rates for hopping steps of different lengths. The significance of *relative*, but not *absolute*, rates for theoretical analysis of steady-state experiments is a direct consequence of two competitive decay channels existing for a positive charge at each step of transport process, namely hole transfer between nearest-neighbor G sites through the AT bridge and irreversible side reaction of the cation G^+ with water.

Knowledge of relative hopping rates, however, is insufficient to describe dynamics of holes generated in DNA and to decide how fast a positive charge can be transferred over a certain distance. To address these kinetic aspects of the problem, data on the absolute rates for each step of the hopping process are required. Although direct measurements of all rates remains a

* To whom correspondence should be addressed.
[†] Arizona State University. E-mail: dmitrym@asu.edu.
[‡] Northwestern University. E-mail: ratner@chem.nwu.edu, berlin@chem.nwu.edu.

10.1021/jp035546x CCC: $25.00
Published on Web 12/02/2003

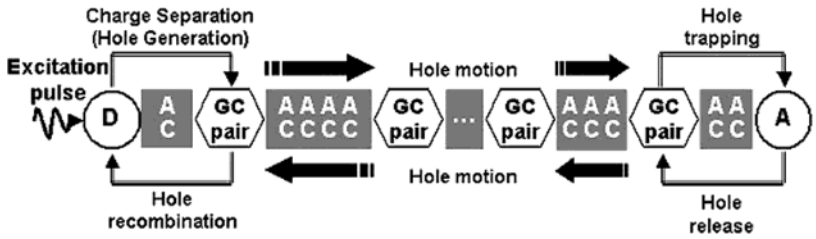

Figure 1. Schematic illustration of model systems and main rate processes with the participation of "electronic holes". Holes are generated due to electron transfer from proximal G base to photoexcited neutral[31,55,57,60,62,64] or positively charged donors,[56,59,61,63] D, incorporated in the stack. Thereafter the primary radical cation G^+ is able to lose its positive charge in several competitive processes. These include hole transfer to the nearest-neighbor neutral G base through the AT bridge (depicted by a black block arrow), recombination due to the positive charge transition from G^+ to D and a side reactions with water. The later process is too slow to be observed in time-resolved experiments and is not shown in the figure. The propagation of a positive charge via series of hops between neighboring G bases continues until a hole has reached a trap, which represents an acceptor molecular unit (A) built in the stack or multiple G sites (usually GG doublet or triple GGG unit) with G bases located on the same strand. Charge transfer between distal G and A can be reversible or can lead to the irreversible disappearance of a hole depending on the nature of the A unit.

challenge for experimentalists, it has been demonstrated that for certain elementary steps, the absolute rate values can be deduced from the results of transient absorption or fluorescent lifetime experiments[55−64] with relatively short duplex DNA oligomers. The model systems investigated and main rate processes involving holes are schematically depicted in Figure 1. Using various oligomeric systems, hole generation, recombination, trapping, and release from the trap were studied within time intervals ranging from femtoseconds to microseconds by probing either the excited-state behavior of the hole-injecting chromophore (as, for example, in ref 56) or an excited nucleobase analogue (for instance 2-aminopurine[55,64]) intercalated at a basic site, or by observation of the charge-transfer intermediate state (as in capped DNA hairpins[57,60,62]).

Similarly to steady-state strand-cleavage experiments, the results of time-resolved studies are usually discussed in terms of nonadiabatic electron-transfer theory,[65,66] assuming that each elementary hopping step can be treated as electron transfer in the direction opposite to the direction of positive charge propagation.[67] Then, the probability of nonadiabatic charge transfer (CT) is a product of the electronic coupling matrix element H_{DA} and the Franck−Condon weighted density of states FCWD

$$k_{CT} = \frac{2\pi}{\hbar}|H_{DA}|^2 \mathrm{FCWD}(\Delta G,\lambda) \tag{1}$$

In eq 1, ΔG is the free energy difference between products and reactants and λ is the reorganization energy for charge transfer.

Equation 1 can be used for comparison of calculated and experimental hopping rates if the values of parameters ΔG, H_{DA}, and λ are known. For elementary steps of hole transport, $\Delta G = 0$ because CT occurs between equivalent sites.[67] If, however, these sites differ, as in the case of hole generation, recombination, trapping, and hole release from the trapping unit A (see Figure 1), the free energy difference can be evaluated at the quantum chemical level.[68,72] Recent calculations of electron coupling, its distance, and conformational dependence[23,40,69,70] also enable one to estimate the H_{DA} values for different duplexes.

Unlike the free energy difference and the electronic coupling matrix element, theoretical evaluations of reorganization energy λ for DNA oligomers are rather rare. Generally, the value of λ is determined by changes in molecular geometry (the inner contribution, λ_v) and by variations in nuclear coordinates of the surrounding medium (the solvent contribution, λ_s). For DNA, the λ_v value was estimated using different quantum chemical methods,[71] whereas λ_s was calculated classically using dielectric continuum models of the aqueous environment.[73−75] In the study by Tavernier and Fayer the reorganization energy is estimated as a sum of longitudinal contributions from dielectric shells of varying dielectric constant around the DNA core. Tong et al.[74] and, more recently, Siriwong et al.[75] reported the electrostatic energy of nuclear reorganization of the transferred charge in a heterogeneous dielectric environment by solving the Poisson equation. In all reported cases, the solvent reorganization energy is predicted to increase smoothly with the donor−acceptor distance in general accord with the Marcus model.[76]

All calculations reported so far predict a very substantial dependence of λ_s on the donor−acceptor distance. This dependence should be included into the overall observed falloff of the rate constant with the donor−acceptor separation R_{DA}

$$k_{CT} \propto e^{-\beta_{DA}R_{DA}} \tag{2}$$

where the falloff parameter

$$\beta_{DA} = \beta_0 + \beta_s \tag{3}$$

is the sum of the contribution β_0 arising from $|H_{DA}|^2$ and the component β_s from the FCWD. In case of charge hops between equivalent sites ($\Delta G = 0$), the falloff parameter β_s originates from the distance dependence of the reorganization energy λ_s. From the classical Marcus equation for the activation energy of charge transfer

$$G^{act} = \frac{(\lambda_s + \Delta G)^2}{4\lambda_s} \tag{4}$$

one gets $\beta_s = \beta_\lambda$ at $\Delta G = 0$, where

$$\beta_\lambda = (1/4k_BT)(\partial\lambda_s/\partial R_{DA}) \tag{5}$$

Here, k_B is Boltzmann's constant and T is the temperature. When classical vibrations of the solute are coupled to CT, the corresponding classical internal reorganization energy λ_v^{cl} adds to λ_s in eq 4. When solute's vibrations are quantum, one has to consider the complete FCWD factor in eq 1. The latter is a sum of individual vibronic excitations each broadened by the inhomogeneous distribution of classical nuclear modes. However, the effect of quantum vibronic excitations is small for CT in the normal region with $\lambda_s + \lambda_v^{cl} < |\Delta G|$ (see below), and eq 5 gives an accurate estimate of β_s at $\Delta G = 0$.

The previous calculations of λ_s[74,75] at varying distance between equivalent G sites lead to $\beta_s \simeq 1.0$ Å^{-1} at $R_{DA} < 15$ Å. Combined with the theoretical calculations of $\beta_0 \simeq 0.7-1.7$ Å^{-1}, this places β_{DA} in the range 1.7−2.7 Å^{-1}. This number is

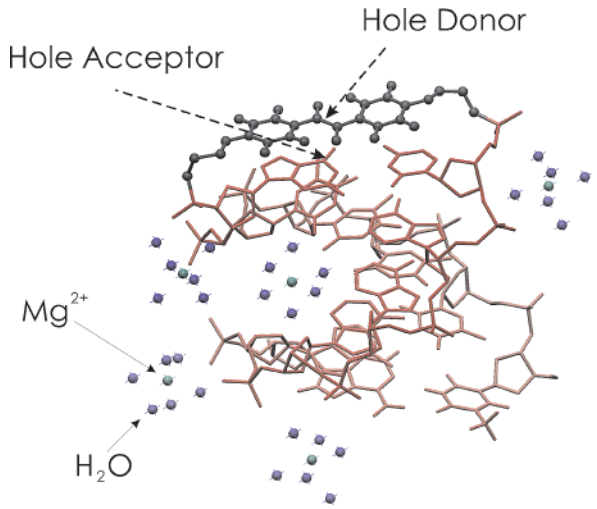

Figure 2. Crystal structure of stilbene diether-linked hairpin with the GC pair located next to the linker.[78] Dashed arrows indicate the centers of electron localization on the linker and N1 nitrogen of G. Also shown are magnesium ions with coordinated water molecules that are considered as bound water in the reorganization energy calculations.

much higher than the experimental falloff parameter $\beta_{DA} \simeq 0.7$ Å^{-1} reported by Lewis et al. for hole injection from stilbene linkers to GC pairs in DNA hairpins[31,77] if one assumes that β_s values for hole generation and hole hopping are close to each other. On the other hand, $\beta_{DA} > 2.0$ Å^{-1} was found for acridine derivatives used as hole donors intercalated in DNA duplexes.[61]

In the present study, we report calculations of the solvent reorganization energies for CT in synthetic DNA hairpins studied by Lewis et al.[31,57,60,62,79] (Figure 2). In contrast to earlier calculations[73−75] based on dielectric solvent models, we employ a molecular-based, nonlocal model of solvent response, and as such this is the first step toward modeling the activation barrier of CT in DNA using microscopic models of solvent reorganization. The microscopic theory is compared to dielectric continuum calculations. We also reanalyze the kinetic CT data[77] within a new model of electron-transfer activation,[80] which accommodates different solvent reorganization energies for charge separation (CS) and charge recombination (CR) reactions. The new model predicts a much weaker dependence of the FCWD on the solvent reorganization energy than what follows from eq 5 so that $\beta_s < \beta_\lambda$. The combination of β_0 from the energy gap analysis with calculated β_s leads to β_{DA} values in reasonable agreement with experiment.

II. Calculation Procedure

The present calculation of the solvent reorganization energy extends the formalism of response functions used in dielectric solvation theories to incorporate the molecular correlation length between orientations of permanent dipoles in water into the calculation of solvation energetics. This is achieved by including the complete dependence of the response function on the inverse-space wave-vector k instead of using the $k = 0$ limit of the dielectric continuum models. This approach aims at two goals. On one hand, we want to achieve a reduced description projecting the many-body manifold of solvent configurations on a few collective modes coupled to the transferred electron. On the other hand, the formalism preserves the molecular length scale of the response. The latter goal is dictated by the desire to accurately include the response of the solvent in confined space encountered in minor and major grooves of DNA molecules. The complete dielectric response may not yet develop when the confinement length is comparable with the correlation length of solvent nuclear fluctuations activating CT. Full k-dependent response functions should account for such situations.

A. Formalism. Solvation of permanent charges in dense polar solvents is well described within the linear response approximation (LRA).[81] In application to the activation of charge-transfer reactions this implies that the donor−acceptor energy gap is a Gaussian stochastic variable leading to the Marcus picture of intersecting parabolas.[65,76,82] The width of the energy gap fluctuations is independent of the charge state of the donor−acceptor complex in the LRA; i.e., it is the same in the initial and final CT states. This property is used here to define λ_s. The reorganization energy is obtained through the variance of the donor−acceptor energy gap ΔV calculated from the configurations of the solvent in equilibrium with a fictitious solute which has all the properties of the real solute but does not include the solute−solvent electrostatic coupling:

$$\lambda_s = \frac{1}{2k_BT}\langle(\delta\Delta V)^2\rangle_0 \tag{6}$$

Here, the subscript "0" in $\langle ... \rangle_0$ indicates that the only influence of the solute on the solvent is to expel it from solute's volume. Physically, this situation corresponds to the initial state of the CS reaction.

The solute−solvent electrostatic interaction is modeled by the charge-dipole potential

$$\Delta V = -\sum_{j=1}^{N} \mathbf{m}_j \cdot \Delta\mathbf{E}_0(\mathbf{r}_j) \tag{7}$$

where $\Delta\mathbf{E}_0(\mathbf{r}_j)$ is the difference of vacuum electric fields of the electron localized on the donor and acceptor. The sum runs over the N solvent molecules with dipole moments $\mathbf{m}_j$ located at the points $\mathbf{r}_j$. For large solutes of the size of the DNA, the interaction of gradients of the solute field with higher solvent multipoles is negligible.[83,84] However, higher multipoles, particularly quadrupoles, affect very significantly the solvent response function (see below).

Equation 6 is written for the interaction of the solute with a nonpolarizable solvent. Solvent polarizability can be included by renormalizing the solvent dipole moment from its gas-phase value m to a condensed-phase value m'.[85−87] This renormalization is usually effectively achieved within self-consistent liquid theories,[88] and we are using the Wertheim 1-RPT formulation[89,90] in the calculations below. The solute−solvent interaction potential has then the same form as in eq 7 with the replacement of $\mathbf{m}_j$ with $\mathbf{m}'_j$.

From eqs 6 and 7 λ_s can be obtained through the average over the orientations of the solvent dipoles. This yields[85,91]

$$\lambda_s = \frac{3y_p}{8\pi}\int \frac{d\mathbf{k}}{(2\pi)^3}|\Delta\tilde{E}_0^L(\mathbf{k})|^2 S^L(k) \tag{8}$$

where

$$y_p = (4\pi/9k_BT)\rho(m')^2 \tag{9}$$

is the density of permanent dipoles in a polar solvent, $\rho = N/\Omega$ is the solvent number density, and $S^L(k)$ is defined below. In eq 8,

$$\Delta\tilde{E}_0^L(\mathbf{k}) = \hat{\mathbf{k}} \cdot \int_\Omega \Delta\mathbf{E}_0(\mathbf{r}) e^{i\mathbf{k}\cdot\mathbf{r}}\, d\mathbf{r} \tag{10}$$

is the longitudinal projection of the Fourier transform of the difference electric field taken over the volume Ω of the solvent. The solvent volume is obtained by excluding the volume Ω_0, which includes all the hard cores of the atoms of the solute and an additional volume obtained by adding the radius $\sigma/2$ to solute atoms exposed to the solvent (σ is the diameter of solvent molecules).

The longitudinal component of the field, obtained as a scalar product of the field Fourier transform with the unit wave-vector $\hat{\mathbf{k}} = \mathbf{k}/k$, enters the equation for λ_s. This means that our present calculations are limited to long-distance CT, when the transverse component of the field and the transverse polarization response are insignificant.[92] Because only the longitudinal component is included in the difference field, the polar solvent response is defined by the longitudinal structure factor[93,94]

$$S^{\mathrm{L}}(k) = \frac{3}{N}\left\langle \sum_{i,j} (\hat{\mathbf{e}}_i \cdot \hat{\mathbf{k}})(\hat{\mathbf{k}} \cdot \hat{\mathbf{e}}_j) \mathrm{e}^{\mathrm{i}\mathbf{k}\cdot\mathbf{r}_{ij}} \right\rangle \tag{11}$$

Here, $\hat{\mathbf{e}}_j$ is the unit vector of the solvent dipole $\mathbf{m}_j$ ($\hat{\mathbf{e}}_j = \mathbf{m}_j/m$) and $\langle ... \rangle$ stands for the statistical average over the configurations of the pure solvent. The structure factor $S^{\mathrm{L}}(k)$ describes correlations of longitudinal (parallel to an external field) fluctuations of the nuclear solvent polarization.[93,94] In the continuum limit of $k = 0$ the structure factor is related to the solvent Pekar factor $c_0 = \epsilon_\infty^{-1} - \epsilon_s^{-1}$ as

$$S^{\mathrm{L}}(0) = c_0/3y_{\mathrm{p}} \tag{12}$$

When the solute size, or the characteristic length of the volume restricting the solvent fluctuations, is much larger than the correlation length Λ_{L} of longitudinal polarization fluctuations, the difference field $\Delta\tilde{E}_0^{\mathrm{L}}(\mathbf{k})$ changes much faster with k than does $S^{\mathrm{L}}(k)$. In this case one can put $S^{\mathrm{L}}(k) \simeq S^{\mathrm{L}}(0)$ in eq 8 with the continuum result

$$\lambda_s = c_0 \mathcal{E}_0^{\mathrm{L}} \tag{13}$$

The longitudinal electrostatic energy in eq 13

$$\mathcal{E}_0^{\mathrm{L}} = (8\pi)^{-1} \int \frac{\mathrm{d}\mathbf{k}}{(2\pi)^3} |\Delta\tilde{E}_0^{\mathrm{L}}(\mathbf{k})|^2 \tag{14}$$

leads to the standard Marcus expression for λ_s[76] when the longitudinal field of two charged spheres is used for $\Delta\tilde{E}_0^{\mathrm{L}}(\mathbf{k})$ in eq 14.[85]

Equation 8 can be generalized to situations when the solvent structure around the solute is inhomogeneous. This includes regions of bound water for aqueous solutions of DNA, the dielectric properties of which may be different from those of the bulk water. We will consider regions of solvent around the solute with volumes Ω_1, ..., Ω_n with Ω_n standing for the bulk solvent (Figure 3). Each solvent region is characterized by its own polarization structure factor $S_i^{\mathrm{L}}(k)$. When polarization fluctuations in each region Ω_i are uncorrelated, the expression for the reorganization energy generalizes to

$$\lambda_s = \frac{3y_{\mathrm{p}}}{8\pi} \sum_{i=1}^{n} \int |\Delta\tilde{E}_i^{\mathrm{L}}(\mathbf{k})|^2 S_i^{\mathrm{L}}(k) \frac{\mathrm{d}\mathbf{k}}{(2\pi)^3} \tag{15}$$

Here,

$$\Delta\tilde{E}_i^{\mathrm{L}}(\mathbf{k}) = \hat{\mathbf{k}} \cdot \int_{\Omega_i} \Delta\mathbf{E}_0(\mathbf{r}) \mathrm{e}^{\mathrm{i}\mathbf{k}\cdot\mathbf{r}}\, \mathrm{d}\mathbf{r} \tag{16}$$

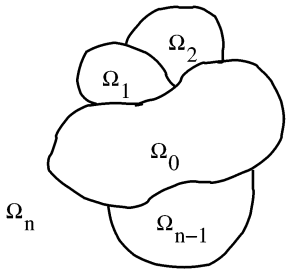

Figure 3. Solvent regions Ω_1, ..., Ω_{n-1} with different dielectric properties around the solute occupying the region Ω_0. Bulk water corresponds to region Ω_n.

is the Fourier transform obtained by integration over the ith solvent region Ω_i. The additive scheme in eq 16 neglects polarization correlations across the heterogeneous boundaries. This approximation is adopted because no information on structure factors and relative effects of cross-correlations in heterogeneous polar media is currently available. Note, that for dielectric models the additive scheme leads to deviations within 15% of the full calculation.[75] It is not clear if the same extent of error should apply to our calculations because the dielectric limit in our scheme gives values for λ_s substantially smaller than the full k integration (see section 3 below).

B. Solvent Parametrization. The representation of the solute−solvent interaction by the charge-dipole potential is based on the assumption of smallness of the ratio l_{ss}/R_{0s} of the distance between the partial charges on the solvent molecules l_{ss} and the characteristic distance R_{0s} between the centers of charge localization on the solute and the solvent molecules. The effective radius of the solute can be estimated from the solute volume Ω_0 as $(4\pi/3){R_{0s}}^3 \simeq \Omega_0$. For the DNA hairpins considered here the assumption $l_{ss}/R_{0s} \ll 1$ is usually well justified ($l_{ss} \simeq 0.38$ Å and $R_{0s} \simeq 13$ Å).[95] The distance R_{0s} also defines the range of decay of the integrand in the k integral in eq 8: $k \leq 2\pi/R_{0s}$. Again, the large size of the solute limits the range of k values significant for the reorganization energy calculations to small k values corresponding to long-range polarization fluctuations of the solvent. From the viewpoint of the calculation of λ_s, this implies that a real solvent can be replaced by a model solvent that reproduces the long-range polarization behavior of the real solvent.

In polar solvents, fluctuations of dipolar polarization have the longest correlation length. One could therefore consider a liquid of point dipoles as a first approximation to calculate the structure factor $S^{\mathrm{L}}(k)$. The replacement of the charge distribution of a real solvent molecule by a point dipole relies, however, on a much weaker assumption than the use of the charge-dipole potential for the solute−solvent coupling. For the point dipoles to reproduce the solvent polarization, the ratio l_{ss}/σ must be small. This rarely happens in dense molecular solvents, and the inclusion of higher point multipoles is necessary for an accurate modeling of the polarization structure factor.

The main problem arising with the use of the model of point dipoles for the calculation of $S^{\mathrm{L}}(k)$ is that solvent molecular quadrupoles strongly affect the solvent dielectric constant[88,96] and therefore $S^{\mathrm{L}}(0)$ (see eq 12). When this effect is incorporated into the parametrization of the structure factor, polar solvents can be successfully described by models developed for purely dipolar solvents. This approach was utilized in parametrized polarization structure factors (PPSF).[92] The PPSF parametrization uses the fact that the mean-spherical approximation (MSA) solution for a dipolar hard-sphere (HS) solvent[97] gives $S^{\mathrm{L}}(k\sigma)$

$$S^{\mathrm{L}}(k\sigma) = |Q(k\sigma)|^{-2} \tag{17}$$

defined by two parameters, a^L and Λ^L, as follows

$$Q(k\sigma) = 1 - 12a^L\int_0^1 e^{ik\sigma t}[(t^2-1)/2 - \Lambda^L(t-1)]\,dt \quad (18)$$

The parameters a^L and Λ^L are related to $S^L(0)$:

$$2a^L(2-3\Lambda^L) = 1/\sqrt{S^L(0)} - 1 \quad (19)$$

Here, Λ^L is the correlation length of the longitudinal polarization fluctuations of the solvent. It can by found within the MSA by solving the following equation for the polarity parameter ξ^L[97]

$$\frac{(1-2\xi^L)^4}{(1+4\xi^L)^2} = S^L(0) \quad (20)$$

The parameter ξ^L is then used in the MSA definition of the longitudinal correlation length[98]

$$\Lambda^L = 3\sigma\xi^L/(1+4\xi^L) \quad (21)$$

With the parameters a^L and Λ^L defined by eqs 19−21 the structure factor $S^L(\kappa k\sigma)$ given by eqs 17 and 18 was used in the calculations, where $\kappa = 0.9$ is an empirical shift used to bring the PPSF in agreement with Monte Carlo computer simulations of pure dipolar solvents.[92]

The Wertheim self-consistent scheme has been used to calculate the effective dipole moment m' and the effective dipolar density y_p (eq 9) of water. This procedure iteratively solves the equation for the dipole moment in the condensed phase renormalized from its gas-phase value m by the self-consistent field of liquid induced dipoles:

$$\mathbf{m'}\cdot[\mathbf{1} - a(m')\boldsymbol{\alpha}] = \mathbf{m} \quad (22)$$

where $\boldsymbol{\alpha}$ is the tensor of the solvent molecular polarizability. The response function $a(m')$ in eq 22 is defined through the average energy of interaction between renormalized dipoles in the pure solvent $u_p(m')$ as follows

$$a(m') = -\frac{1}{m'}\frac{\partial u_p(m')}{\partial m'} \quad (23)$$

The energy $u_p(m')$ in eqs 22 and 23 is taken in the Padé form proposed by Stell et al.[99,100]

The longitudinal polarization structure factor is parametrized in our calculations by six solvent properties: two dielectric constants, ϵ_∞ and ϵ_s, the solvent number density ρ, the gas-phase dipole moment $m = 1.87$ D, molecular polarizability $\alpha = 1.47$ Å^3, and molecular diameter $\sigma = 2.87$ Å. The first five properties are experimentally determined; the solvent diameter is tabulated from fitting the experimental compressibility of water to the equation of state for the fluid of dipolar HS molecules.[101] The Wertheim procedure[89] used in our calculations gives $m' = 2.43$ D, which agrees well with the value $m' = 2.35-2.65$ D from computer simulations and ab initio calculations.[102]

C. Energy Gap Law. The calculations of the reorganization energy are supplemented by the analysis of the energy gap law for the kinetic data reported by Lewis et al.[77] The analysis of the dependence of the rate constant on the free energy gap ΔG (energy gap law) is usually performed using the Marcus−Levich−Jortner (MLJ) equation[41,103]

$$k_{CT} = \frac{2\pi}{\hbar}|H_{DA}|^2\sum_{n=0}^{\infty} e^{-S}\frac{S^n}{n!}G(\Delta G + \lambda_s + n\hbar\omega_v) \quad (24)$$

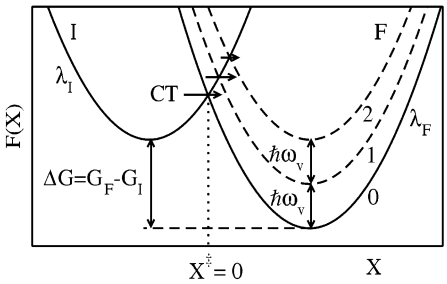

Figure 4. Free energy surfaces $F(X)$ for CT from the initial state I to the final state F. 0, 1, 2 indicate vibrational excitations of the solute in its final CT state. The free energy gap is defined as the difference in equilibrium free energies in the final and initial states. The reaction coordinate X refers to the donor−acceptor energy gap with $X^\ddagger = 0$ corresponding to the activated state.

where $G(X)$ is a Gaussian distribution of the energy gap variable X

$$G(X) = [4\pi k_B T\lambda_s]^{-1/2}e^{-X^2/4k_BT\lambda_s} \quad (25)$$

In eq 24, $S = \lambda_v/\omega_v$ is the Huang−Rhys factor and ω_v is the average frequency of solute's normal mode vibrations.

The appearance of the Gaussian distribution in eq 24 is a part of the Marcus−Hush picture of CT based on the assumption that the donor−acceptor energy gap is a Gaussian stochastic variable. Several physical reasons may account for non-Gaussian statistics of the energy gap: nonlinear solvation,[104,105] conformational flexibility,[80,106] polarizability changes,[80,107,108] and transfer from unrelaxed excited states have been considered in the literature. Independently of a physical reason of non-Gaussian statistics, one needs a consistent extension of eqs 24 and 25 to take these effects into account. This is achieved by the Q-model of CT,[80,107,108] which provides a consistent, nonphenomenological approach to calculate the free energy surfaces of CT in cases of nonequal reorganization energies for the initial and final CT states. The energy gap distributions are given in terms of non-Gaussian functions

$$P(X) = \sqrt{\frac{\lambda_I|\alpha_I|^3}{|X|}}\frac{1}{k_BT(1-e^{-\alpha_I^2\lambda_I/k_BT})}e^{-(\alpha_I|X|+\alpha_I^2\lambda_I)/k_BT}\times I_1(2\sqrt{\lambda_I|\alpha_I|^3|X|}/k_BT) \quad (26)$$

where $I_1(x)$ is the first-order modified Bessel function[109] and the subscript "I" refers to the initial state of the particular CT processes under consideration. The equation for the energy gap law then becomes

$$k_{CT} = \frac{2\pi}{\hbar}|H_{DA}|^2\sum_{n=0}^{\infty} e^{-S}\frac{S^n}{n!}P\left(\Delta G - \lambda_I\frac{\alpha_I^2}{\alpha_F} + n\hbar\omega_v\right) \quad (27)$$

The CT reaction discussed here is illustrated in Figure 4. The reaction proceeds from the initial state (I) with the classical reorganization energy λ_I to the final state (F) with the reorganization energy λ_F. For CS reactions, I = CS, $\lambda_I = \lambda_{CS}$, and $\lambda_F = \lambda_{CR}$. For the backward CR transition, I = CR, $\lambda_I = \lambda_{CR}$, and $\lambda_F = \lambda_{CS}$. In each case, the free energy gap is the difference in final and initial free energies (Figure 4). The two reorganization energies are defined in terms of the curvatures of the free energy surfaces evaluated at their corresponding minima

$$\lambda_{CS/CR} = \frac{1}{2k_B T}\langle(\delta X)^2\rangle_{CS/CR} \quad (28)$$

Equations 26 and 27 fully define the energy gap law in term of three parameters: driving force ΔG and two solvent reorganization energies, λ_{CS} and λ_{CR}. The nonparabolicity parameter $\alpha_{CS/CR}$ quantifies the distinction between the curvatures of the CS and CR free energy surfaces at their minima:

$$\alpha_{CS} = (\sqrt[3]{\lambda_{CS}/\lambda_{CR}} - 1)^{-1} \quad (29)$$

and

$$\alpha_{CR} = 1 + \alpha_{CS} \quad (30)$$

When $\lambda_{CS} \rightarrow \lambda_{CR}$, $\alpha_{CS/CR} \rightarrow \infty$ and eq 27 transforms to eq 24 with $\lambda_{CS} = \lambda_{CR} = \lambda_s$.

Figure 4 also shows the vibrationally excited states of the solute in its final CT state. When the temperature is small compared to the spacing between the vibronic free energy surfaces $\hbar\omega_v$, the CT reaction proceeds from the vibrationally ground state (one surface for state I, Figure 4). Vibronic states labeled $n = 0, 1, 2, \ldots$ to which the transition can occur correspond to summation over separate vibronic channels in eqs 24 and 27. In the normal CT region, states with $n > 0$ have higher activation energy, and only $n = 0$ effectively contributes to the rate. Therefore, the use of the complete FCWD factor for the calculation of CT rates in the CT normal region turns out to be numerically equivalent to using just classical expressions for the activation barrier along the reaction coordinate X (see section 4 below).

D. Numerical Procedure. The calculations of the solvent reorganization energy were carried out for two types of CT transitions studied experimentally: hole ejection from a photoexcited stilbene linker and hole hopping between two G sites connected by $(AT)_n$ bridges of different length. The SE-linked SE(G:C)(T:A)$_5$ hairpin (SE = stilbene diether, Figure 2) with the known structure[78] was used as the basis for generating eleven hairpins. In the first set of six hairpins denoted by nG:C (n = 1, ..., 6, Figure 5) the position of the only GC pair is systematically increased from $R_{DA} = 3.4$ up to 20.1 Å. By contrast, the second set of five hairpins denoted by n,6G:C (n = 2, ..., 6) contain duplexes with two GC pairs. One of these pairs is always at the end of the stack (position 6), whereas the location of the other can be shifted from the position adjacent to the SE linker to the position adjacent to the first GC pair. New DNA molecules were created from the initial structural file[78] by using the InsightII molecular modeling system.[110] Hydrogens were added using the Biopolymer module, and the potential of each atom was assigned by DISCOVER module. The nucleotide-replace feature of the Biopolymer module was utilized to mutate the 1G:C hairpin to each of the corresponding molecules. After this mutation, the geometry of each molecule was minimized using the steepest descent algorithm.

The molecular cores of the hairpins were obtained by assigning van der Waals atomic radii according to the parametrization by Banavali and Roux.[111] To form the volume excluded by the solute from the solvent, the radius $\sigma/2$ of water ($\sigma = 2.87$ Å[101]) was added to each atom. The sum of the atomic and solvent radii constitutes the closest distance a point dipole of the solvent can approach the solute. The hole was localized at N1 nitrogen of G involved in deprotonation in aqueous solution.[112−114] The difference electric field $\Delta\mathbf{E}_0(\mathbf{r})$ (see eq 7) was created by placing a positive charge on the hole acceptor (G) and a negative charge on the hole donor. For hole hopping, the second G with variable position in the strand serves as the donor. For hole injection the center of the electronic charge distribution was placed on the carbon−carbon double bond between two rings of stilbene diether linker (Figure 2). The Fourier transform of the difference field outside the DNA molecule was calculated by fast Fourier transform (FFT)[115] and then used for the integration with the polarization structure factor in eq 8.

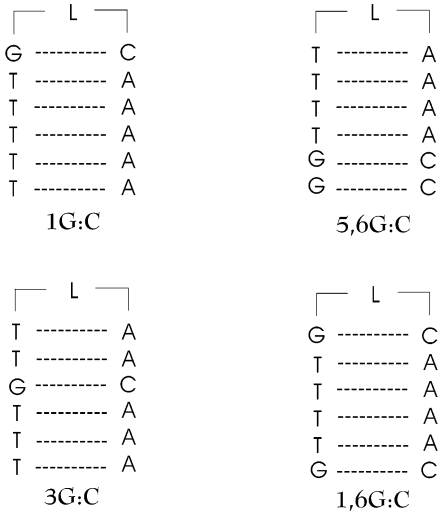

Figure 5. Examples of SE-linked DNA hairpins (L = SE) and their nomenclature.

TABLE 1: Solvent Parameters Used in the Calculations[a]

region	calculation	ϵ_s	ϵ_∞	m, D	σ, Å	η[b]
1	I	1.78	1.78	0	2.87	0.413
1	II	78.3	1.78	1.83	2.87	0.413
2	I + II	78.3	1.78	1.83	2.87	0.413

[a] Regions 1 and 2 correspond to bound and bulk water, respectively. [b] $\eta = (\pi/6)\rho\sigma^3$.

The calculation of the solvent component of the classical reorganization energy presents a significant challenge due to dielectric heterogeneity of water close to the DNA surface.[117,118] To account for partial immobilization of water, the dielectric constants 20 and 55 have been assigned in the literature to the minor and major grooves of the DNA, respectively.[117] The spatial extent of these regions is not well-defined, and the present calculations are based solely on the experimental structural data. They indicate regions of bound water coordinated to magnesium ions fixed in the structural data close to phosphate groups of the DNA backbone (Figure 2). Dielectric properties of coordinated water are unknown, and we performed calculations for two limiting sets of dielectric constants: in set I the bound water (region 1) was completely immobilized ($\epsilon_s = \epsilon_\infty = 1.78$, Table 1) and in set II the bound water was considered a part of the bulk solvent (region 2, $\epsilon_s = 78.3$, Table 1). We assume that restrictions on orientational mobility of water molecules imposed by coordination to magnesium ions affect only the dielectric constant (through the Kirkwood factor[119]) and do not affect the density (computer simulations show that this may not be true[118]). The calculations indicate a very small effect of coordinated water on λ_s (see below), and approximations adopted for the dielectric properties of this region should not be critical for our analysis. No mobile counterions (Na^+) have been included in the reorganization energy calculations. The static electric field of the counterions does not contribute to the solvent reorganization energy built on the difference of electric fields in the final and initial CT states (eq 8). Thermal fluctuations of the self-

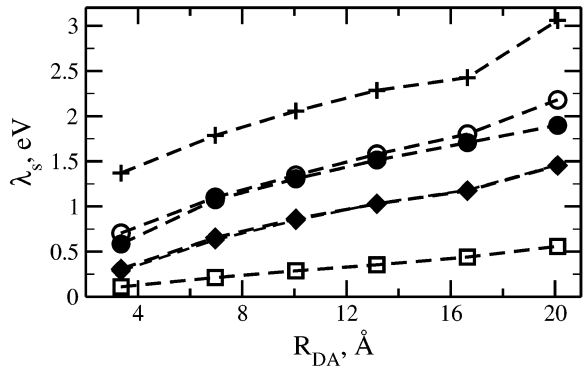

Figure 6. λ_s for CS in the 1G:C−6G:C hairpins vs the distance between the linker and G, R_{DA}. Calculations are performed according to eq 15 with bound water assigned properties of the bulk (open circles, set of parameters I in Table 1) and with completely immobilized bound water (closed circles, set of parameters II in Table 1). Squares refer to to the continuum limit of eq 15 when the structure factor is replaced by $S^L(0)$ (eqs 12 and 13). Diamonds are Delphi[116] calculations in sets of parameters I and II when the dielectric cavity is defined through the solvent-accessible surface. The two Delphi calculations (diamonds) almost coincide on the plot scale. Crosses refer to DelPhi calculations with the standard definition of the dielectric cavity through the van der Waals surface.

consistent Debye−Hückel field may have a contribution to the solvent reorganization energy in the limit of slow CT,[120] but are unlikely to have any significant effect of fast CT with $k_{ET} \simeq 10^9$ s^{-1} considered here.

In the production calculations we used a cubic grid of 512 × 512 × 512 points with the distance between the grid points of 0.37 Å (6G:C hairpin). This size choice is dictated by the balance between the necessity to minimize the errors of the numerical FFT procedure arising from induced periodicity when FFT is performed on a finite box[115] and to produce a sufficient density of points in the inverted **k** space for the calculation of the integral in eq 8. The details of the calculation algorithm are presented elsewhere.[92]

III. Calculation Results

We report here the calculation of the *solvent* reorganization energy only and do not consider nuclear reorganization arising from classical motions of the DNA backbone. Dielectric constants of <5 and ≃30 are usually assigned to the base and phosphate regions, respectively,[117] to account for high conformational mobility of molecular groups within DNA molecules. The dielectric continuum calculations then include nuclear reorganization arising from thermal librations of polar molecular groups within DNA in terms of their continuum polarization. It is not currently clear how accurate these estimates may be because direct calculations of the reorganization energy arising from phosphate groups give negligible contributions.[71]

All dielectric continuum calculations performed on DNA duplexes so far report quite significant reorganization energies of the order of 1.0−2.0 eV for CT between G sites.[73−75] In addition, all calculations give a significant falloff parameter β_λ of the order of 1.0 Å^{-1} at R_{DA} < 15 Å.[75] On the other hand, solvent reorganization energies of the order of 0.2 eV with no significant distance dependence were inferred from the MLJ energy gap analysis by Lewis et al.[77]

The previous calculations of the reorganization energy were performed on DNA duplexes that do not include intercalated or hairpin-bound chromophores used in experiment for hole generation. Our present calculations explicitly consider solutes with stilbene linkers, and therefore directly apply to kinetic data obtained on synthetic hairpins by Lewis et al.[77] Figure 6 shows the dependence of λ_s on R_{DA} for charge injection from the SE linker to G in *n*G:C hairpins. The reorganization energy is about 0.7 eV for 1G:C when no bound water is present in the solvent. It drops to 0.58 eV (Table 2) when water coordinated to magnesium ions is excluded from the solvent nuclear polarization response. Overall, the effect of coordinated water on λ_s is relatively small. This may be explained by the fact that regions of magnesium-coordinated water are relatively distant from the centers of charge localization (Figure 2) accounting for only a small fraction of the total electrostatic energy.

The results of calculations with nonlocal polarization response (eq 15) were compared to dielectric continuum calculations using the Poisson equation solver DelPhi.[116] Two approaches were used to define the dielectric cavity. First, we used van der Waals atomic radii[111] to form the van der Waals surface followed by the DelPhi smoothing procedure producing the molecular surface.[121] This procedure, usually employed in dielectric calculations,[74,75] gives the highest values for λ_s obtained in this study (crosses in Figures 6 and 7). We also used the solvent-accessible surface, which is obtained by adding the solvent radius to the van der Waals radii. The reorganization energies are then substantially smaller (diamonds in Figures 6 and 7). In fact, the results of explicit-solvent calculations (circles in Figures 6 and 7) fall between the two types of dielectric calculations. On the qualitative side, the DelPhi calculations support the very low sensitivity of the reorganization energy to the presence of coordinated water (the results of calculations with and without coordinated water coincide on the scale of Figure 6). The results for hole transfer between G's in *n*,6G:C hairpins (Figure 7) are qualitatively similar to the results on hole injection. In this later case λ_s values from the nonlocal formalism are closer to DelPhi results with the solvent-accessible definition of the cavity (cf. circles and diamonds in Figure 7), and again, there is only a minor effect of coordinated water on λ_s.

The slope of the dependence of λ_s on R_{DA} does not change much between different sets of calculations reflecting the fundamental electrostatic nature of this variation. The falloff parameter β_λ (eq 5) calculated from the polarization structure factor is about 1.0 Å^{-1} in going from 1G:C to 3G:C in *n*G:C hairpins and is equal to 0.6 Å^{-1} in going from 5,6G:C to 3,-6G:C in *n*,6G:C hairpins (Table 2). The standard DelPhi calculations (set II^b in Table 2) give $\beta_\lambda = 1.0$ Å^{-1} for 1G:C−3G:C and $\beta_\lambda = 1.2$ Å^{-1} for 5,6G:C−3,6G:C. The latter value is twice as high as what follows from our molecular-response calculations. Despite this disagreement, the present results essentially reinforce the conclusions of previous dielectric calculations concerning the magnitude of the reorganization energy falloff parameter.[74,75] The magnitudes of the solvent reorganization energies obtained here are, however, much smaller than those in standard dielectric continuum calculations. A substantial portion of λ_s calculated according to eq 15 comes from the nonlocal nature of the solvent response given in terms of the *k*-dependent structure factor $S^L(k)$. Squares in Figures 6 and 7 refer to the continuum limit of eq 15 when the structure factor in the *k* integral is replaced by its $k = 0$ value, $S^L(0)$. This is the limit employed in the calculations by Tavernier and Fayer.[73] The gap between circles and squares in Figures 6 and 7 accounts for the nonlocal part of the solvent response not included in dielectric calculations.

Our values for reorganization energies are more than twice as high as the values obtained from the MLJ energy gap analysis (eq 24). λ_s from the MLJ analysis is also much smaller than one normally observes for CT complexes dissolved in water.

TABLE 2: Solvent Reorganization Energy for Hole Injection from SE Linker into the *n*G:C Hairpins and for Hole Hopping between Neighboring GC Pairs in the *n*,6G:C Hairpins

		λ_s, eV						λ_s, eV			
hairpin	R_{DA}	I	II[1]	II[2]	II	hairpin	R_{DA}	I	II[a]	II[b]	II
1G:C	3.35	0.58	0.29	1.37	0.71	5,6G:C	3.6	0.27	0.23	0.75	0.30
2G:C	6.96	1.07	0.63	1.79	1.10	4,6G:C	6.9	0.59	0.50	1.32	0.61
3G:C	10.1	1.31	0.85	2.06	1.35	3,6G:C	10.1	0.78	0.71	1.58	0.77
4G:C	13.2	1.51	1.03	2.29	1.56	2,6G:C	13.2	0.94	0.89	1.84	0.98
5G:C	16.6	1.71	1.18	2.43	1.80	1,6G:C	16.8	1.21	1.07	2.02	1.26
6G:C	20.1	1.90	1.46	3.06	2.18						

[a] DelPhi calculation with the solvent-accessible surface used as the dielectric cavity. [b] DelPhi calculation with the van der Waals surface used as the dielectric cavity.

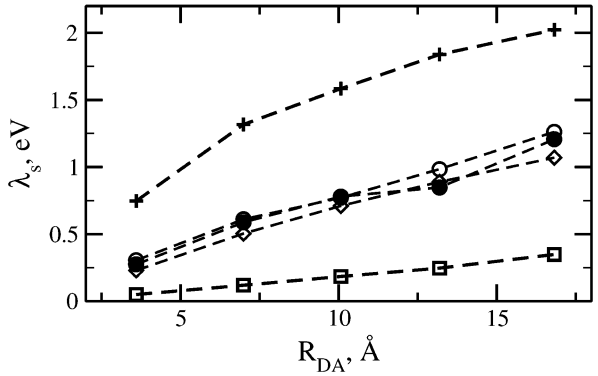

Figure 7. λ_s for hole hopping between two G bases in 1,6G:C−5,-6G:C hairpins. Note that R_{DA} corresponds to the distance between two Gs. For other notation, see caption to Figure 6. Open diamonds refer to the set of parameters I with solvent-accessible cavity.

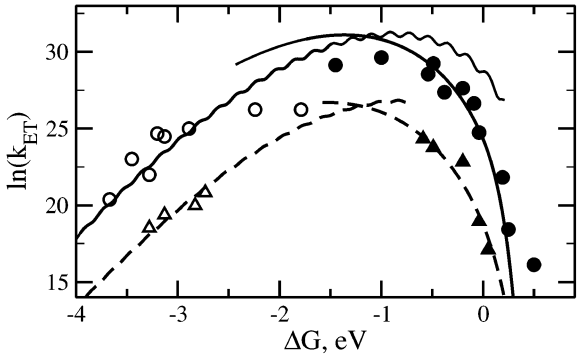

Figure 8. Dependence of CT rate constant for CS (closed points) and CR (open points) on the free energy gap ΔG for 1G:C (circles) and 3G:C (up-triangles) hairpins. Lines are global fits of the experimental rates[77] for 1G:C (solid lines) and 3G:C (dashed lines) to the Q model energy gap law (eq 27). The distinction between each of pairs of solid or dashed lines reflects the difference in reorganization energies for CS and CR reactions.

An explanation of this result may be sought in unusual dielectric properties of water on the surface of DNA molecules. Structuring of water on the surface of DNA[117,122] is the basis of applying multizone models for dielectric electrostatic calculations. In the absence of direct experimental evidence on the polarization properties of surface water, significant uncertainties remain concerning the construction of multizone dielectric layers. The present calculations are based on the experimental structural information that provides only the regions of magnesium-coordinated water. No change in the polarization response of interfacial water is thus included. Recent measurements by Berg and co-workers[123] for coumarin-102 intercalated in a DNA duplex have shown Stokes shifts close to values measured in the aqueous solution of coumarin-102. The dielectric environment of an intercalated chromophore is thus only slightly less polar than that of a chromophore in the bulk water. This experimental observation gives some support to our calculations' neglecting possible changes in water polarization response arising from DNA grooves and allows us to suggest that the solvent reorganization energy must be much higher than what follows from the MLJ analysis.

To reconcile the calculations of the solvent reorganization energy with the experimentally measured rate constants, we have performed an energy gap analysis of the CS and CR rate constants reported by Lewis et al.[77] for SA-linked hairpins (SA = stilbenedicarboxamide). The analysis is carried out in the framework of the Q-model allowing more flexibility of choosing the activation parameters.[80] The main difference compared to the MLJ analysis is the recognition of the possibility of different solvent reorganization energies for CS and CR reactions. As a result, the free energy surfaces are significantly asymmetric even without the inclusion of the vibrational intramolecular excitations. Figure 8 shows the results of the global fit (using both CS and CR data for one set of fitted values, simulated annealing technique[115]) of CS and CR rate constants to eq 27 with four fitting parameters: λ_{CS}, λ_{CR}, λ_v, and H_{DA} ($\hbar\omega_v = 1500$ cm^{-1}). The results are compared to the MLJ analysis in Table 3.

TABLE 3: Electron-Transfer Parameters from the Global Fit of Experimental CS and CR Rate Constants[77] to Eq 27

system	method	λ_{CS}, eV	λ_{CR}, eV	λ_v, eV	H_{DA}, cm^{-1}	α_{CS}
1G:C	MLJ[1]	0.23	0.23	0.99	347	
1G:C	Q-Model	0.54	0.1	1.14	518	1.33
3G:C	MLJ[1]	0.27	0.27	1.03	25	
3G:C	Q-Model	0.85	0.13	1.17	58	1.15

[a] Results from ref 77.

The intramolecular reorganization energy from the fit as listed in Table 3 is higher than what is usually encountered for intramolecular CT in organic donor−acceptor complexes. The reorganization energy λ_v can be split into two components: the energy of removing one electron from G, λ^+, and the energy for adding one electron to the linker, λ^-. The first component is known from experiment, $\lambda^+ = 0.47$ eV.[71] The energy of placing an extra electron on a stilbene linker is unknown, but based on quantum-mechanical calculations of this quantity for simpler molecules,[124] one can expect that λ^- is in the same range as λ^+. In this case the total reorganization energy becomes close to the values reported in Table 3.[74]

The fitting parameters listed in Table 3 indicate the possibility of a significant anisotropy between the CS and CR reorganization energies. The clear distinction between each of two solid (1G:C) and dashed (3G:C) lines is a manifestation of the fact that the energy gap laws are not equivalent for CS and CR reactions in the Q-model. In the case when polarizability change is responsible for deviations from the MLJ picture, the difference between λ_{CS} and λ_{CR} is caused by the polarization of the donor−acceptor complex by the reaction field of the solvent in response

to a large dipole in the final charge-transfer state. When the solute field is represented by point dipoles, the reorganization energy of polarized donor−acceptor complex becomes[107]

$$\lambda_{CS/CR} \simeq \lambda_s\left[1 - 2\Delta F_{p,CS/CR}\frac{\Delta\alpha_0}{\Delta m_0^2}\right] \qquad (31)$$

where $\Delta\alpha_0$ and Δm_0 are polarizability and dipole moment change, respectively, and $\Delta F_{p,CS/CR}$ is the shift of the vertical CT transition energy induced by the nuclear polarization of the solvent. For the initial neutral state this term is insignificant and $\lambda_{CS} \simeq \lambda_s$. The fitted CS reorganization energies indeed agree well with the calculations: 0.54 from the second row in Table 3 vs 0.58 and 0.71 eV from the first row in Table 2. [No perfect match is expected as the kinetic data and calculations refer to different linkers, SA and SE, respectively.[125]] The charge-separated state creates a large dipole moment resulting in a red shift, $\Delta F_{p,CR} < 0$. The reorganization energy λ_{CR} may then become smaller than λ_{CS} if the charge transition leads to a reduction in the polarizability of the hairpin molecule, $\Delta\alpha_0 < 0$.

Equations 24 and 27 apply to nonadiabatic CT when the electronic coupling H_{DA} is significantly smaller than the vertical energy gap for the transition: $\Delta G + n\hbar\omega_v + \lambda_s$ in the MLJ formalism and $\Delta G + n\hbar\omega_v + \alpha_I\lambda_I/\alpha_F$ in the Q-model. The relatively large values of H_{DA} for 1G:C from the fit (Table 3) make points on top of the bell-shaped curve a suspect. For these points, the activation barrier should be reduced by H_{DA},[126] and the downward deviation for both CS and CR rates in the region near the top is not surprising. Note also that the closed circle in the right corner of Figure 8 is not known with sufficient accuracy[77] and was excluded from the fit.

IV. Discussion

Recent computational and experimental studies of CT in DNA present a puzzling problem for the interpretation of kinetic measurements for the distance falloff of hole-transfer rate constants. For transitions in the normal region with $\lambda > |\Delta G|$ the MLJ formalism predicts that the falloff parameter β_s is mostly a result of the distance dependence of ΔG and λ, which reduces to $\beta_s = \beta_\lambda$ (eq 5) for hops between G sites. Both previous dielectric calculations on DNA duplexes and our present results on DNA hairpins place β_λ in the range ≤ 1.0 Å^{-1} for $R_{DA} < 10.1$ Å. The resultant $\beta_{DA} \simeq 1.7-2.7$ Å^{-1} is then much higher than the value of $\beta_{DA} \simeq 0.7-0.9$ Å^{-1} in Lewis et al.[31,77] experiments. The calculated solvent reorganization energy also turned out to be inconsistent with the MLJ analysis of the energy gap law. We found, however, that the calculations can be reasonably well reconciled with experiment when the energy gap law is analyzed within the Q-model.[80] This success poses the question whether the apparent inconsistencies between measured and calculated β_{DA} may be attributed to a failure of the MLJ scheme. In particular, a too strong dependence of the Franck−Condon factor on λ_s may be responsible for too high values of calculated β_s.

Both large-amplitude conformational motions altering the donor−acceptor distance and variations in the dipolar polarizability result in bilinear dependence ($\propto P_n + aP_n^2$) of the donor and acceptor electronic energies on the nuclear polarization of the solvent P_n.[80,127,128] On the contrary, the MLJ formalism assumes a linear coupling ($\propto P_n$) of the donor and acceptor energy levels to P_n, leading to the Gaussian statistics of the donor−acceptor energy gap. It is reasonable to expect that both the polarizability change and alterations of the donor−acceptor distance may occur in DNA molecules.[129] Independently of the underlying physical mechanism, the bilinear solute−solvent coupling causes a significant asymmetry of the charge-transfer free energy surfaces, superimposed with asymmetry that may arise from intramolecular vibrational excitations. Asymmetry of the charge-transfer free energy surfaces along the solvent reaction coordinate is controlled by the nonparabolicity parameter $\alpha_{CS/CR}$. This parameter also controls the sensitivity of the activation barrier G^{act} to changes in the driving force and solvent reorganization energy. The Q-model activation barrier along the classical reaction coordinate X is given by the expression[80]

$$G^{act} = |\alpha_I|(\sqrt{|\Delta G - \lambda_I\alpha_I^2/\alpha_F|} - \sqrt{|\alpha_I|\lambda_I})^2 \qquad (32)$$

At $\alpha_{I/F} \rightarrow \infty$ the above equation transforms into the Marcus formula (eq 4), as can be demonstrated by the series expansion of the first square root in eq 32 in $1/\alpha_{I/F}$ and using the connection in eq 30 between α_{CS} and α_{CR}.

The Marcus equation (eq 4) predicts that G^{act} changes with λ_s with the slope 0.25 at $\Delta G = 0$ (dashed lines in Figure 9). The slope extracted from eq 32 is, however, much smaller (solid lines in Figure 9) at $\alpha_{CS} \simeq 1$, resulting from the analysis of experimental kinetic data (Table 3). The results of calculations of the parameter β_s within different sets of data and using the MLJ and Q-model formalisms are summarized in Table 4. To have a clear comparison between the molecular-based and continuum calculations of λ_s, calculation set II from Table 2 was used. As mentioned above, the use of either the equations for the activation barrier (eqs 4 and 32) or the complete FCWD (eqs 24 and 27) does not significantly affect β_s for charge-transfer reactions in the normal region. Despite close magnitudes

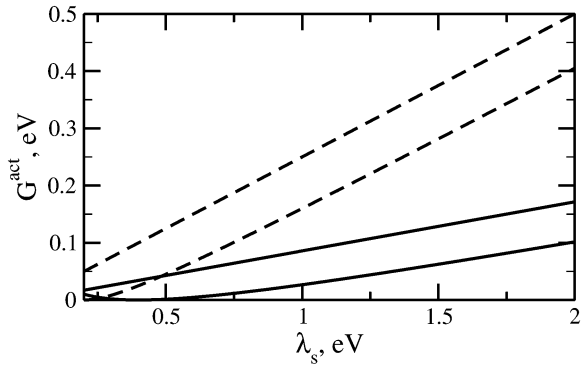

Figure 9. Dependence of the activation energy of CT on λ_s according to the Marcus equation (dashed lines, eq 4) and from the Q model (solid lines, eq 32). The upper and lower lines refer to $\Delta G = 0$ and $\Delta G = -0.2$ eV, respectively; $\alpha_1 = 1.0$ in the Q model calculations.

TABLE 4: Calculated Values of the Fall-off Parameter β_s

		β_s,[a] Å^{-1}			β_s,[b] Å^{-1}		
system	ΔG, eV	I[c]	II[d]	III[e]	I[f]	II[g]	III[h]
1G:C-3G:C	−0.2	0.90	0.26	0.99	0.89	0.32	0.99
5,6G:C-3,6G:C	0.0	0.56		1.16	0.60		1.17

[a] Calculated from the activation energy along the solvent reaction coordinate, eqs 4 and 32. [b] Calculated from the FCWD from eqs 24 and 27; $\omega_v = 1500$ cm^{-1}, $\lambda_v = 0.97$ eV. [c] λ_s from set II in Table II in combination with the Marcus equation, eq 4. [d] λ_s from set II in Table II with the Q model expression for the activation barrier along the solvent reaction coordinate, eq 32. [e] λ_s from DelPhi calculations in set II in Table II in combination with the Marcus equation, eq 4. [f] λ_s from set II in Table II in combination with the MLJ formula, eq 24. [g] λ_s from set II in Table II with the Q model form for the FCWD, eq 27. [h] λ_s from DelPhi calculations in set IIb in Table II in combination with the MLJ formula, eq 24.

of β_λ in all sets of calculations, the resultant β_s is strongly model-dependent: the MLJ formalism predicts much higher magnitudes for β_s compared to the Q-model. Specifically, at $\alpha_{CS} = 1.33$ and $\Delta G = -0.2$ eV[77] the change in λ_s from 0.7 eV for 1G:C to 1.35 eV for 3G:C results in $\beta_s = 0.32$ Å^{-1}, much smaller than $\beta_s = 1$ Å^{-1} following from the MLJ analysis (following ref 77, we assume that ΔG does not change between 1G:C and 3G:C). With $\beta_0 \simeq 0.66$ Å^{-1} from the fitting parameters in Table 3, this estimate yields $\beta_{DA} = 0.98$ Å^{-1}, in a reasonable agreement with experimental $\beta_{DA} = 0.7-0.9$ Å^{-1}.[77]

A possibility of proton transfer across the GC pair may affect the result of reorganization energy calculations. The multistep processes of deprotonation of $G^{+\cdot}$ occurs on the time scale of microseconds.[114] This is much slower than the time of hole injection $\simeq 10^{-9}$ s for hairpins considered here.[77] However, the elementary step of proton transfer along the hydrogen bond connecting N1 of G and N3 of C may be very fast. One therefore needs to assume a possibility of changing the hole location. The equilibrium constant for proton transfer, $pK_{eq} = 2.5$, suggests that the hole is predominantly localized on G. Nevertheless, a partial delocalization of the positive charge may affect the calculation of λ_s. Changing the hole location from N1 of G to N3 of C predominantly affects λ_s for hairpins with the GC pair close to stilbene. For instance, moving the hole from N1 of G to N3 of C changes R_{DA} from 3.35 to 4.7 Å for 1G:C, from 6.96 to 7.8 Å for 2G:C, and from 10.1 to 10.7 Å for 3G:C. A partial shift of the hole to C is thus expected to weaken the dependence of λ_s on R_{DA}, bringing the falloff parameter in closer agreement with experiment.

The solvent reorganization energies calculated here can be used to determine the absolute rate of hole transfer between G sites. Lewis et al.[57] report rate constants $\simeq 5 \times 10^7$ and $\simeq 6 \times 10^6$ s^{-1}, respectively, for the forward and backward hole transfer between G and GG across a single A base. The electronic coupling through a single A is given by Olofsson and Larsson as $H_{DA}(G-A-G^+) = 1.2 \times 10^{-2}$ eV and $\beta_0 = 1.30$ Å^{-1} (DFT calculations) for the $G-A_n-G^+$ strand.[71] The ratio of the forward and backward rates yields $\Delta G = -0.054$ eV. The 5′-G in the GG site is more readily oxidized,[130,131] and one can assume that the hole transfers to the closest G in the GG pair. The reorganization energy can then be estimated as that for 4,-6G:C from column 1 in Table 2 ($\lambda_s = 0.59$ eV). Quantum intramolecular vibrations, which are assumed to be the only source of intramolecular reorganization in this paper, do not affect the charge-transfer rate in the normal region of CT (Figure 4). Therefore, the direct application of eq 1 with the activation energy in the form of eq 4 (assuming no asymmetry in reorganization parameters between charges on G and GG) gives for the forward rate 2×10^{10} s^{-1}. In case when the GG site is flanked by two A bases, as is in $3G_3$ hairpin of Lewis et al,[57] the hole charge is equally distributed between two G bases in the GG site.[131] With the above value of β_0, this gives $H_{DA} = 1.3 \times 10^{-3}$ eV. The reorganization energy for this configuration can be estimated by taking the mean of reorganization energies for 4,6G:C and 3,6G:C in column 1 in Table 2. This estimate yields $\lambda_s \simeq 0.69$ eV, leading to the forward rate constant 7×10^7 s^{-1}, which compares well with the experimental value reported by Lewis et al.[57]

The present calculations of the solvent reorganization energy combine the explicit crystallographic information on the structure of the DNA solute with an explicit solvent model given in terms of the *k*-dependent polarization structure factors. This feature of the model allows us to include the nonlocal character of the solvent response. The crystallographic data identify regions of immobilized water coordinated to magnesium ions in the solution. Our calculations, however, show a very minor effect of these regions on the solvent reorganization energy. Water located in minor and major grooves of DNA molecules may have polarization responses different from those of the bulk solvent.[73−75,117,118] In the absence of direct experimental evidence on the dielectric properties and spacial extent of these regions in molecules under study, we have resolved not to change dielectric properties of water in DNA grooves compared to the bulk solvent. This approximation may account for slightly higher values of the calculated reorganization energies compared to those extracted from experimental kinetic data (cf. Tables 2 and 3).

An interesting observation following from the present calculations is a substantial effect of the nonlocal character of the solvent response on the magnitude of λ_s. The value of the reorganization energy obtained by full integration of the polarization structure factor with the difference electric field $|\Delta\tilde{E}_0(\mathbf{k})|^2$ (eq 8) is substantially higher than the continuum estimate obtained by assuming that $S^L(k) \simeq S^L(0)$ does not change with *k* (cf. circles and squares in Figures 6 and 7). Complex geometry of the double helix may be partially responsible for this effect. The minor and major grooves of the double helix have length scales much smaller than the characteristic size of the whole molecule. These length scales create a nonzero component of $|\Delta\tilde{E}_0(\mathbf{k})|^2$ at relatively large *k* values for which the polarization structure factor starts to rise as a reflection of nonlocal polarization correlations in water. The total *k* integral is then much higher than its value obtained with the continuum estimate $S^L(k) \simeq S^L(0)$. Note, however, that the region of *k* integration significant for the reorganization energy calculation is still much smaller than the values of the wave vector at which the multipolar expansion becomes invalid and accounts for the finite distance between the partial charges on the solvent molecules become necessary.[132]

V. Summary

This study presents a consistent analysis of the experimental results on the hole injection from stilbene linkers to DNA hairpins. We report the first calculation of the solvent reorganization energy of charge transfer in DNA fragments based on the nonlocal, molecular-based description of the solvent response. The calculated reorganization energies, although different in magnitude from dielectric calculations, give a similar falloff parameter with the donor−acceptor distance. Combined with theoretical and experimental estimates of the falloff of the electronic coupling, these results give too strong, compared to experiment, overall decay of the charge-transfer rate constant when either the Marcus or, more generally, the MLJ formalism is applied. The controversy is resolved by the application of the new model (Q-model), which predicts a much lower sensitivity of the overall rate constant to changes in the solvent reorganization energy than traditional theories. When the Q-model is applied to experimental kinetic data, the calculated and fitted values of the solvent reorganization energy are in good agreement. The study highlights possible limitations of the MLJ formalism in application to CT in asymmetric charge-transfer systems and stresses the necessity of molecular-based modeling of solvent reorganization in CT.

Acknowledgment. We are grateful to the Research Corporation and ACF-PRF (D.V.M.), the Chemistry Divisions of the NSF, ONR, and the DoD/MURI Program (M.A.R. and Yu.A.B.) for support. This is publication No. 559 from the ASU

Photosynthesis Center. We thank Prof. F. Lewis for sharing the spectroscopic data on DNA hairpins and useful discussions.

References and Notes

(1) Murphy, C. J.; Arkin, M. R.; Jenkins, Y.; Ghatlia, N. D.; Bossman, S. H.; Turro, N. J.; Barton, J. K. *Science* **1993**, *262*, 1025.
(2) Arkin, M. R.; Stemp, E. D. A.; Holmlin, R. E.; Barton, J. K.; Hormann, A.; Olson, E. J. C.; Barbara P. F. *Science* **1996**, *273*, 475.
(3) Hall, D. B.; Holmlin, R. E.; Barton J. K. *Nature* **1996**, *382*, 731.
(4) Armitage, B. *Chem. Rev.* **1998**, *98*, 1171.
(5) Burrows, C. J.; Muller, J. G. *Chem. Rev.* **1998**, *98*, 1109.
(6) Guallar, V.; Douhal, A. Moreno, M.; Lluch, J. M. *J. Phys. Chem. A* **1999**, *103*, 6251.
(7) Loft, S.; Poulsen, H. E. *J. Mol. Med.* **1996**, *74*, 297.
(8) Demple, B.; Harrison, L. *Annu. Rev. Biochem.* **1994**, *63*, 915.
(9) Boon, E. M.; Ceres, D. M.; Drummond, T. G.; Hill, M. G.; Barton, J. K. *Nature Biotechnol.* **2000**, *18*, 1096.
(10) Hartwich, G.; Garuana, C. J.; de Lumley-Woodyear, T.; Wu, Y.; Campbell, C. N.; Heller, A. *J. Am. Chem. Soc.* **1999**, *121*, 10803.
(11) Lisdat, F.; Ge, B.; Scheller, F. W. *Electrochem. Commun.* **1999**, *1*, 65.
(12) Porath, D.; Bezryadin, A.; de Vries, S.; Dekker, C. *Nature* **2000**, *403*, 635.
(13) Storhoff, J. J.; Mirkin C. A. *Chem. Rev.* **1999**, *99*, 1849.
(14) Fink, H.-W.; Schonenberger, C. *Nature* **1999**, *398*, 407.
(15) Winfree E.; Liu, F.; Wenzler, L. A.; Seeman, N. C. *Nature* **1998**, *394*, 539.
(16) Braun, E.; Eichen, Y.; Sivan, U.; Ben-Joseph, G. *Nature* **1998**, *391*, 775.
(17) Okata, Y.; Kobayashi, T.; Tanaka, K.; Shimomura, M. *J. Am. Chem. Soc.* **1998**, *120*, 6165.
(18) Alivisatos, A. P.; Johnson, K. P.; Wilson, T. E.; Loveth, C. J.; Bruchez, M. P.; Schultz, P. G. *Nature* **1996**, *382*, 609.
(19) Mirkin, C. A.; Letsinger, R. L.; Mucic, R. C.; Stofhoff, J. J. *Nature* **1996**, *382*, 607.
(20) Cai, Z. L.; Li, X. F.; Sevilla, M. D. *J. Phys. Chem. B* **2002**, *106*, 2755.
(21) Behrens, C.; Burgdorf, L. T.; Schwgler, A.; Carell, T. *Angew. Chem., Int. Ed.* **2002**, *41*, 1763.
(22) Li, X. F.; Cai, Z. L.; Sevilla, M. D. *J. Phys. Chem. A* **2002**, *106*, 1596.
(23) Voityuk, A. A.; Michel-Beyerle, M. E.; Rösch, N. *Chem. Phys. Lett.* **2001**, *342*, 231.
(24) Cai, Z.; Gu, Z.; Sevilla, M. D. *J. Phys. Chem. B* **2000**, *104*, 10406.
(25) Cai, Z.; Sevilla, M. D. *J. Phys. Chem. B* **2000**, *104*, 6942.
(26) Messer, A.; Carpenter, K.; Forzley, K.; Buchanan, J.; Yang, S.; Razskazovskii, Y.; Cai, Z.; Sevilla, M. D. *J. Phys. Chem. B* **2000**, *104*, 1128.
(27) Berlin, Y. A.; Kurnikov, I. V.; Beratan, D.; Ratner, M. A.; Burin, A. L. In *Topics in Current Chemistry*; Schuster, G. B., Ed. (submitted for publication).
(28) Giese, B. *Annu. Rev. Biochem.* **2002**, *71*, 51.
(29) Boon, E. M.; Barton, J. K. *Curr. Opin. Struct. Biol.* **2002**, *12*, 320.
(30) Dekker, C.; Ratner, M. A. *Phys. World* **2001**, *14*, 29.
(31) Lewis, F. D.; Letsinger, R. L.; Wasielewski, M. R. *Acc. Chem. Res.* **2001**, *34*, 159.
(32) Giese, B. *Acc. Chem. Res.* **2000**, *33*, 631.
(33) Schuster, G. B. *Acc. Chem. Res.* **2000**, *33*, 253.
(34) Grinstaff, M. W. *Angew. Chem., Int. Ed. Eng.* **1999**, *38*, 3629.
(35) Turro, N. J.; Barton, J. K. *JBIC, J. Biol. Inorg. Chem.* **1998**, *3*, 201.
(36) Diederichsen, U. *Angew. Chem., Int. Ed. Eng*. **1997**, *36*, 2317.
(37) Steenken, S. *Biol. Chem.* **1997**, *378*, 1293.
(38) Seidel, C. A. M.; Schultz, A.; Sauer, M. H. M. *J. Phys. Chem.* **1996**, *100*, 5541.
(39) Steenken, S.; Jovanovic, S. V. *J. Am. Chem. Soc*. **1997**, *119*, 617.
(40) Voityuk, A. A.; Jortner, J.; Bixon, M.; Rösch, N. *Chem. Phys. Lett.* **2000**, *324*, 430.
(41) Jortner, J.; Bixon, M.; Langenbacher, T.; Michel-Beyerle, M. E. *Proc. Natl. Acad. Sci. U.S.A.* **1998**, *95*, 12759.
(42) Meggers, E.; Michel-Beyerle, M. E.; Giese, B. *J. Am. Chem. Soc*. **1998**, *120*, 12950.
(43) Ratner, M. A. *Nature* **1999**, *397*, 480.
(44) Giese, B.; Amaudrut, J.; Khler, A.-K.; Spormann, M.; Wessely, S. *Nature* **2001**, *412*, 318.
(45) Berlin, Y. A.; Burin, A. L.; Ratner, M. A. *Chem. Phys.* **2002**, *275*, 61.
(46) Bixon, M.; Jortner, J. *Chem. Phys.* **2002**, *281*, 393.
(47) Henderson, P. T.; Jones, D.; Hampikian, G.; Kan, Y. Z.; Schuster G. B. *Proc. Natl. Acad. Sci. U.S.A.* **1999**, *96*, 8353.
(48) Giese, B.; Wessely, S.; Spormann, M.; Lindemann, U.; Meggers, E.; Michel-Beyerle, M. E. *Angew. Chem., Int. Ed. Engl.* **1999**, *38*, 996.
(49) Bixon, M.; Giese, B.; Wessely, S.; Langenbacher, T.; Michel-Beyerle, M. A.; Jortner, J. *Proc. Natl. Acad. Sci. U.S.A.* **1999**, *96*, 11713.
(50) Berlin, Y. A.; Burin, A. L.; Ratner, M. A. *J. Phys. Chem. A* **2000**, *104*, 443.
(51) Bixon, M.; Jortner, J. *J. Phys. Chem. B* **2000**, *104*, 3906.
(52) Berlin, Y. A.; Burin, A. L.; Ratner, M. A. *J. Am. Chem. Soc*. **2001**, *123*, 260.
(53) Yu, Z. G.; Song X. Y. *Phys. Rev. Lett.* **2001**, *86*, 6018.
(54) O'Neill, P.; Fielden, E. M. *Adv. Radiat. Biol.* **1993**, *17*, 53.
(55) Wan, C.; Fiebig, T.; Kelley, S. O.; Treadway, C. R.; Barton, J. K.; Zewail, A. H. *Proc. Natl. Acad. Sci. U.S.A.* **1999**, *96*, 6014.
(56) Fukui, K.; Tanaka, K.; Fujitsuka, M.; Watanabe, A.; Ito, O. J. *Photochem. Photobiol. B* **1999**, *50*, 18.
(57) Lewis, F. D.; Liu, X.; Liu, J.; Miller, S. E.; Hayes, R. T.; Wasielewski, M. R. *Nature* **2000**, *406*, 51.
(58) Shafirovich, V.; Dourandin, A.; Huang, W.; Luneva, N. P.; Geacintov, N. E. *Phys. Chem. Chem. Phys.* **2000**, *2*, 4399.
(59) Davis, W. B.; Naydenova, I.; Haselsberger, R.; Ogrodnik, A.; Giese, B.; Michel-Beyerle, M. E. *Angew. Chem., Int. Ed.* **2000**, *39*, 3649.
(60) Lewis, F. D.; Liu, X.; Liu, J.; Hayes, R. T.; Wasielewski, M. R. *J. Am. Chem. Soc.* **2000**, *122*, 12037.
(61) Hess, S.; Gotz, M.; Davis, W. B.; Michel-Beyerle, M. E. *J. Am. Chem. Soc.* **2001**, *123*, 10046.
(62) Lewis, F. D.; Zuo, X.; Liu, J.; Hayes, R. T.; Wasielewski, M. R. *J. Am. Chem. Soc*. **2002**, *124*, 4568.
(63) Davis W. B.; Hess S.; Naydenova, I.; Haselsberger, R.; Ogrodnik, A.; Newton, M. D.; Michel-Beyerle, M. E. *J. Am. Chem. Soc.* **2002**, *124*, 2422.
(64) Fiebig, T.; Wan, C. Z.; Zewail, A. H. *ChemPhysChem* **2002**, *3*, 781.
(65) Marcus, R. A.; Sutin, N. *Biochim. Biophys. Acta* **1985**, *811*, 265.
(66) Bixon, M.; Jortner, J. *Adv. Chem. Phys.* **1999**, *106*, 35.
(67) The same approach is shown to be useful for the description of hopping transport in molecular wires composed of alternating conjugated and bonded structural units, see: Berlin, Yu. A.; Hutchison, G. R.; Rampala, P.; Ratner, M. A.; Michl, J. *J. Phys. Chem. A*, in press.
(68) Kurnikov, I. V.; Tong, G. S. M.; Madrid, M.; Beratan, D. N. *J. Phys. Chem. B* **2002**, *106*, 7.
(69) Grozema, F. C.; Siebbeles, L. D. A.; Berlin, Y. A.; Ratner, M. A. *ChemPhysChem* **2002**, *3*, 536.
(70) Voityuk, A. A.; Rösch, N. *J. Phys. Chem. B* **2002**, *106*, 3013.
(71) Olofsson, J.; Larsson, S. *J Phys. Chem. B* **2001**, *105*, 10398.
(72) Sugiyama, H.; Saito, I. *J. Am. Chem. Soc.* **1996**, *118*, 7063.
(73) Tavernier, H. L.; Fayer, M. D. *J. Phys. Chem. B* **2000**, *104*, 11541.
(74) Tong, G. S. M.; Kurnikov, I. V.; Beratan, D. N. *J. Phys. Chem. B* **2002**, *106*, 2381.
(75) Siriwong, K.; Voityuk, A. A.; Newton, M. D.; Rösch, N. *J. Phys. Chem. B* **2003**, *107*, 2595.
(76) Marcus, R. A. *Rev. Mod. Phys.* **1993**, *65*, 599.
(77) Lewis, F. D.; Kalgutkar, R. S.; Wu, Y.; Liu, X.; Liu, J.; Hayes, R. T.; Miller, S. E.; Wasielewski, M. R. *J. Am. Chem. Soc.* **2000**, *122*, 12346.
(78) Lewis, F. D.; Liu, X.; Wu, Y.; Miller, S. E. *J. Am. Chem. Soc.* **1999**, *121*, 9905.
(79) Lewis, F. D.; Liu, J.; Zuo, X.; Hayes, R. T.; Wasielewski, M. R. *J. Am. Chem. Soc.* **2003**, *125*, 4850.
(80) Matyushov, D. V.; Voth, G. A. *J. Chem. Phys.* **1999**, *113*, 5413.
(81) Kuharski, R. A.; Bader, J. S.; Chandler, D.; Sprik, M.; Klein, M. L.; Impey, R. W. *J. Chem. Phys.* **1988**, *89*, 3248.
(82) Marcus, R. A. *J. Phys. Chem.* **1989**, *93*, 3078.
(83) Matyushov, D. V.; Voth, G. A. *J. Chem. Phys.* **1999**, *111*, 3630.
(84) Matyushov, D. V.; Newton, M. D. *J. Phys. Chem. A* **2001**, *105*, 8516.
(85) Matyushov, D. V. *Chem. Phys.* **1993**, *174*, 199.
(86) Bader, J. S.; Berne, B. J. *J. Chem. Phys.* **1996**, *104*, 1293.
(87) Bader, J. S.; Cortis, C. M.; Berne, B. J. *J. Chem. Phys.* **1997**, *106*, 2372.
(88) Stell, G.; Patey, G. N.; Høye, J. S. *Adv. Chem. Phys.* **1981**, *18*, 183.
(89) Wertheim, M. S. *Mol. Phys.* **1979**, *37*, 83.
(90) Venkatasubramanian, V.; Gubbins, K. E.; Gray, C. G.; Joslin, C. C. *Mol. Phys.* **1984**, *52*, 1411.
(91) Matyushov, D. V. *Mol. Phys.* **1993**, *79*, 795.
(92) Matyushov, D. V. *J. Chem. Phys.*, submitted for publication.
(93) Madden, P.; Kivelson, D. *Adv. Chem. Phys.* **1984**, *56*, 467.
(94) Raineri, F. O.; Resat, H.; Friedman, H. L. *J. Chem. Phys.* **1992**, *96*, 3068.
(95) The charge is distributed asymmetrically in the hairpins, but the condition for the application of the charge-dipole potential holds for the systems studied here.
(96) Carnie, S. L.; Patey, G. N. *Mol. Phys.* **1982**, *47*, 1129.
(97) Wertheim, M. S. *J. Chem. Phys.* **1971**, *55*, 4291.
(98) Chan, D. Y. C.; Mitchell, D. J.; Ninham, B. W. *J. Chem. Phys.* **1979**, *70*, 2946.

(99) Stell, G. Fluids with long-range forces; Toward a simple analytic theory. In *Statistical Mechanics. Part A: Equilibrium Techniques*; Berne, B. J., Ed.; Plenum: New York, 1977.
(100) Gray, C. G.; Gubbins, K. E. *Theory of molecular liquids*; Clarendon Press: Oxford, U.K., 1984.
(101) Schmid, R.; Matyushov, D. V. *J. Phys. Chem.* **1995**, *99*, 2393.
(102) Ferenczy, G. G.; Reynolds, C. A. *J. Phys. Chem. A* **2001**, *105*, 11470.
(103) Bixon, M.; Jortner, J. *Adv. Chem. Phys.* **1999**, *106*, 35.
(104) Fonseca, T.; Ladanyi, B. M. *J. Mol. Liq.* **1994**, *60*, 1.
(105) Geissler, P. L.; Chandler, D. *J. Chem. Phys.* **2000**, *113*, 9759.
(106) Gierschner, J.; Mack, H.-G.; Lüer, L.; Oekrug, D. *J. Chem. Phys.* **2002**, *116*, 8596.
(107) Matyushov, D. V.; Voth, G. A. *J. Phys. Chem. A* **1999**, *103*, 10981.
(108) Small, D. W.; Matyushov, D. V.; Voth, G. A. *J. Am. Chem. Soc.* **2003**, *125*, 7470.
(109) Abramowitz, M. Stegun, I. A., Eds. *Handbook of mathematical functions*; Dover: New York, 1972.
(110) MSI. "InsightII User Guide", San Diego, 1995.
(111) Banavali, N. K.; Roux, B. *J. Phys. Chem. B* **2002**, *106*, 11026.
(112) Giese, B. *Acc. Chem. Res.* **2000**, *33*, 631.
(113) Weatherly, S.; Yang, I. V.; Armistead, P. A.; Thorp, H. H. *J. Phys. Chem. B* **2003**, *107*, 372.
(114) Kobayashi, K.; Tagawa, S. *J. Am. Chem. Soc.* **2003**, *125*, 10213.
(115) Press: W. H.; Teukolsky, S. A.; Vetterling, W. T.; Flannery, B. P. *Numerical recipes in Fortran 77: The art of scientific computing*; Cambridge University Press: Cambridge, U.K., 1996.
(116) Rocchia, W.; Alexov, E.; Honig, B. *J. Phys. Chem. B* **2001**, *105*, 6507.
(117) Young, M. A.; Jayaram, B.; Beveridge, D. L. *J. Phys. Chem. B* **1998**, *102*, 7666.
(118) Guarnieri, F.; Mezei, M. *J. Am. Chem. Soc.* **1996**, *118*, 8493.
(119) Böttcher, C. J. F. *Theory of electric polarization*; Elsevier: Amsterdam, 1973.
(120) Vakarin, E. V.; Holovko, M. F.; Piotrowiak, P. *Chem. Phys. Lett.* **2002**, *363*, 7.
(121) Rocchia, W.; Sridharan, S.; Nicholls, A.; Alexov, E.; Chiabrera, A.; Honig, B. *J. Comput. Chem.* **2002**, *23*, 128.
(122) Shui, X.; McFail-Isom, L.; Hu, G. G.; Williams, L. D. *Biochemistry* **1998**, *37*, 8341.
(123) Brauns, E. B.; Madaras, M. L.; Coleman, R. S.; Murphy, C. J.; Berg, M. A. *J. Am. Chem. Soc.* **1999**, *121*, 11644.
(124) Berlin, Y. A.; Hutchison, G. R.; Rempala, P.; Ratner, M. A.; Michl, J. *J. Phys. Chem. A* **2003**, *107*, 3970.
(125) The reorganization energy calculations have been performed on hairpins with the SE linker because this is the only synthetic hairpin used in kinetic measurements for which crystallographic structure is available.
(126) Brunschwig, B. S.; Sutin, N. *Coord. Chem. Rev.* **1999**, *187*, 233.
(127) Matyushov, D. V.; Voth, G. A. New developments in the theoretical description of charge-transfer reactions in condensed phases. In *Reviews in computational chemistry*, Vol. 18; Lipkowitz, K. B., Boyd, D. B., Eds.; Wiley-VCH: New York, 2002.
(128) A bilinear dependence of the energy gap on normal modes vibrations of the solute appears in classical studies of radiationless transitions caused by vibrational excitations/relaxation, see: (a) Kubo, R.; Toyozawa, Y. *Prog. Theor. Phys.* **1955**, *13*, 160. (b) Fischer, S. F.; vanDuayne, R. P. *Chem. Phys.* **1977**, *26*, 9. A similar bilinear coupling effect is characteristic of Duschinski rotations, see: Lin, S. H. *J. Phys. Chem. B* **1999**, *103*, 10674. The *Q* model considers a physically different origin of the bilinear coupling arising from a nonlinear dependence of the electronic energies of the transferred electron on the solvent electric field, which can be expressed in terms of linear and higher order solute polarizability.
(129) Voityuk, A. A.; Siriwong, K.; Rösch, N. *Phys. Chem. Chem. Phys.* **2001**, *3*, 5421.
(130) Nakatani, K.; Dohno, C.; Saito, I. *J. Am. Chem. Soc.* **1999**, *121*, 10854.
(131) O'Neill, P.; Parker, A. W.; Plumb, M. A.; Siebbeles, L. D. A. *J. Phys. Chem. B* **2001**, *105*, 5283.
(132) Raineri, F. O.; Friedman, H. L. *Adv. Chem. Phys.* **1999**, *107*, 81.